Applications in Engineering Science 18 (2024) 100181

Contents lists available at ScienceDirect

Applications in Engineering Science

journal homepage: www.elsevier.com/locate/apples

Analytical solution of the Poiseuille flow of a De Kee viscoplastic fluid

Alexandros Syrakos [a,*], Aggelos Charalambous [a], Georgios C. Georgiou [b]

[a] Department of Mechanical and Manufacturing Engineering, University of Cyprus, P.O. Box 20537, 1678 Nicosia, Cyprus
[b] Department of Mathematics and Statistics, University of Cyprus, PO Box 20537, 1678, Nicosia, Cyprus

ARTICLE INFO

Keywords:
Viscoplasticity
De Kee model
Poiseuille flow
Lambert function

ABSTRACT

We provide an explicit analytical solution of the planar Poiseuille flow of a viscoplastic fluid governed by the constitutive equation proposed by De Kee and Turcotte (1980). Formulae for the velocity and the flow rate are derived, making use of the Lambert W function. It is shown that a solution does not always exist because the flow curve is bounded from above and hence the rheological model can accommodate stresses only up to a certain limit. In fact, the flow curve reaches a peak at a critical shear rate, beyond which it exhibits a negative slope, giving rise to unstable solutions.

1. Introduction

Viscoplastic fluids are characterised by the property of behaving in a solid-like manner when the applied stress is below a limit value called the yield stress (Coussot, 2017; Balmforth et al., 2014). Examples of such fluids include toothpaste, hair gel, mayonnaise, shaving foam, mud, mucus, clay, fresh concrete, crude oil, and many others. This class of fluids includes a variety of materials such as foams, emulsions, colloids, and physical gels, with the emergence of yield stress as a macroscopic property being attributable to a variety of microscopic mechanisms, possibly different for each material type (Bonn et al., 2017).

Mathematical modelling of the rheological behaviour of viscoplastic fluids is a field that has been developing during the last century or so. Classic viscoplastic models originate in the work of Eugene Bingham who proposed the famous constitutive model that carries his name (Bingham, 1922). These models, commonly called *simple yield stress fluids*, assume the material to have a solid state that is completely rigid, and a fluid state which is that of a generalised Newtonian fluid. The most popular such model, which incorporates both a yield stress and shear thinning or thickening, is the Herschel–Bulkley (HB) model (Herschel and Bulkley, 1926):

$$\begin{cases} \dot{\gamma} = 0 & \tau < \tau_0 \\ \underline{\underline{\tau}} = \left(\dfrac{\tau_0}{\dot{\gamma}} + k\dot{\gamma}^{n-1} \right) \underline{\underline{\dot{\gamma}}} & \tau \geq \tau_0 \end{cases} \tag{1}$$

where $\underline{\underline{\dot{\gamma}}}$ is the rate-of-strain tensor and $\dot{\gamma} = (\underline{\underline{\dot{\gamma}}} : \underline{\underline{\dot{\gamma}}}/2)^{1/2}$ is its magnitude, $\underline{\underline{\tau}}$ is the deviatoric stress tensor and $\tau = (\underline{\underline{\tau}} : \underline{\underline{\tau}}/2)^{1/2}$ is its magnitude, τ_0 is the yield stress, k is the consistency index, and the exponent n determines the intensity of shear-thinning ($n < 1$) or shear-thickening ($n > 1$). For $n = 1$ the Herschel–Bulkley model reduces to the Bingham model. Another popular model of this class is the Casson model (Casson, 1959).

Real viscoplastic fluids exhibit additional rheological properties such as elasticity and thixotropy (Dinkgreve et al., 2017; Larson and Wei, 2019), a fact that has given rise to recent efforts for the development of more complicated rheological models with expanded physics (Saramito, 2009; Dimitriou and McKinley, 2019; Varchanis et al., 2019). Nevertheless, simple yield stress fluids continue to be used at present and will most likely persist in the future, having the advantages of simplicity and focus on plasticity and shear-thinning, which are the defining aspects of many flows of interest. A recent defence of this class of rheological models is provided by Frigaard (2019).

Simple yield stress fluids are challenging from mathematical and computational perspectives. The stress tensor is indeterminate in the unyielded (solid-state) regions, while the evolution of the yield surfaces (the boundaries between the yielded and unyielded material) is not described explicitly by some equation. Several numerical methods have been developed for solving the flows of simple yield stress fluids (Mitsoulis and Tsamopoulos, 2017; Saramito and Wachs, 2017; Moschopoulos et al., 2022), some of which solve the original models directly while others first regularise them, effectively converting the unyielded material into a very viscous fluid (something that may also have some physical justification, at least for some materials). The most popular regularisation method is that of Papanastasiou (Papanastasiou, 1987).

* Corresponding author.
E-mail address: syrakos.alexandros@ucy.ac.cy (A. Syrakos).

https://doi.org/10.1016/j.apples.2024.100181
Received 5 January 2024; Received in revised form 2 March 2024; Accepted 15 April 2024
Available online 17 April 2024

A less popular simple yield stress fluid model was proposed by De Kee and Turcotte (De Kee and Turcotte, 1980):

$$\begin{cases} \dot{\gamma} = 0 & \tau < \tau_0 \\ \underline{\underline{\tau}} = \left(\dfrac{\tau_0}{\dot{\gamma}} + \eta_1 e^{-t_1 \dot{\gamma}} \right) \underline{\underline{\dot{\gamma}}} & \tau \geq \tau_0 \end{cases} \tag{2}$$

Compared to the Herschel–Bulkley model (1), instead of the consistency k and the power-law exponent n, the De Kee model employs constants η_1 and t_1 which have units of viscosity and time, respectively. For our analysis, it is convenient to define also the reciprocal of the time constant as $\dot{\gamma}_1 = t_1^{-1}$, which has dimensions of strain rate, because, as will be shown, this is a critical value of strain-rate that delimits distinct regions where the properties of the model differ drastically. Like the Herschel–Bulkley model, the De Kee model can predict both plasticity and shear-thinning.

In a later work (Zhu et al., 2005), De Kee and co-workers presented a Papanastasiou-type regularised version of the model in order to bound the viscosity at vanishing shear rate. Since the viscous component $\eta_1 e^{-t_1 \dot{\gamma}}$ is already bounded – which is an advantage of the De Kee model over the HB model – the regularisation needs to be applied only to the plastic component $\tau_0/\dot{\gamma}$ (nevertheless, it should be pointed out that the HB viscosity is easily bounded by applying the regularisation also to the viscous component $k\dot{\gamma}^{n-1}$ (Sverdrup et al., 2018; Syrakos et al., 2020)). Another advantage of the De Kee model is that the dimensions of its constants, η_1 and t_1, are fixed, and they have a clear physical significance, in contrast to the HB parameters where the dimensions of the consistency k depend on n.

The De Kee–Turcotte model has been used in various experimental and numerical studies. Kaczmarczyk et al. (2023) fitted the model (2), incorporating additional viscous terms $\eta_2 e^{-t_2 \dot{\gamma}}$ and $\eta_3 e^{-t_3 \dot{\gamma}}$, to rheological measurements for *Plantago ovata* water extract solutions. They examined both dilute (zero yield stress) and semi-dilute (non-zero yield stress) solutions. Yahia and Khayat (2001) made rheological measurements on cement grout and found that the De Kee model is suitable for mixtures made of 100% cement and rheology-modifying admixtures. Seo et al. (2011) proposed a generalised model for electrorheological fluids which reduces to the De Kee–Turcotte model for particular choices of parameters. The regularised version of the model (Zhu et al., 2005) was used by Zare and Rhee (2019) to model polymer blends and nanocomposites containing poly (lactic acid), poly (ethylene oxide) and carbon nanotubes. In numerical studies, the model was used for the numerical simulation of the cessation of viscoplastic Couette flow (Zhu and De Kee, 2007) and the numerical simulation of the flow in a rheometer with concentric cylinder geometry (Wang et al., 2011).

The present work exposes an inherent limitation of the model: it only yields solutions within limited parameter ranges. This limitation is due to its excessive shear thinning. As an application, we will solve analytically the planar Poiseuille flow and determine the range of parameters for which a solution exists. The solution is obtained with the use of the Lambert W function (Corless et al., 1996), which has proved quite useful in non-Newtonian fluid mechanics. This function is briefly presented in Section 2. The aforementioned limitation of the model is exposed in Section 3, and the analytical solutions, both stable and unstable, of planar Poiseuille flow are presented in Section 4.

2. The Lambert W function

Our analytical solution makes use of the Lambert W function, which returns the solution, in terms of y, of the equation $ye^y = x$, where x is some real number:

$$y\,e^y = x \;\Leftrightarrow\; y = W(x) \tag{3}$$

The function is plotted in Fig. 1. It is multivalued in the interval $(-1/e, 0)$, and therefore consists of two branches: the principle branch, denoted by $W_0(x)$, for $x \in [-1/e, \infty)$, and the secondary branch, denoted as $W_{-1}(x)$, for $x \in [-1/e, 0)$. These branches are illustrated in Fig. 1; the principal branch is strictly increasing from -1 to infinity, while the secondary branch is strictly decreasing from -1 to minus infinity. It is important to note that Eq. (3) does *not* have a solution for $x < -1/e$ and hence $W(x)$ is not defined for $x < -1/e$.

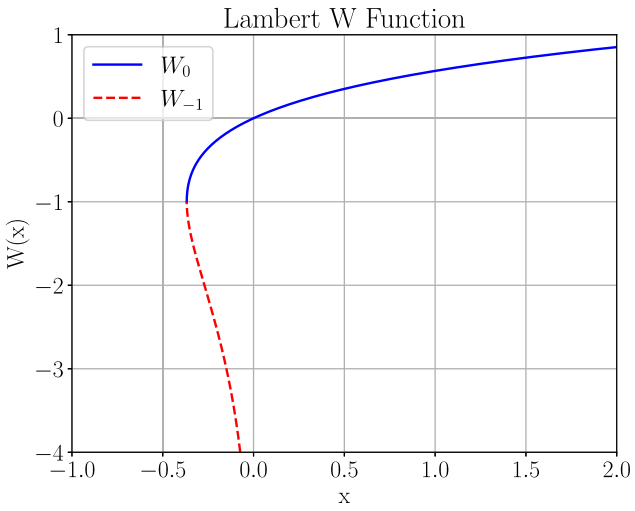

Fig. 1. The Lambert W function, with its two branches, W_0 and W_{-1}.

An overview of the Lambert W function and its applications can be found in Corless et al. (1996). The function is useful in Newtonian fluid mechanics (Pitsillou et al., 2020b), and more so in non-Newtonian fluid mechanics where it has many applications (Pitsillou et al., 2020a; Huilgol and Georgiou, 2022).

Some integrals involving the Lambert function that are useful for the present application are:

$$\int W(x)\,dx = x\,W(x) - x + e^{W(x)} + c \tag{4}$$

$$\int x\,W(x)\,dx = \frac{1}{8}\left(2W(x)^2 + 1\right)(2W(x) - 1)\,e^{2W(x)} + c \tag{5}$$

$$\int e^{W(x)}\,dx = \frac{1}{4}(1 + 2W(x))\,e^{2W(x)} + c \tag{6}$$

where c is an arbitrary constant of integration. All of these expressions can be obtained by making the substitution $W(x) = v \Leftrightarrow ve^v = x \Rightarrow dx = e^v(1+v)dv$, and then repeatedly performing integration by parts.

3. Flow curve

Figs. 2 and 3 illustrate the variation of stress and viscosity, respectively, with shear rate, for the De Kee–Turcotte model. Plot 2 is obtained by taking the norm of Eq. (2). In plot 3 only the "viscous" part, $\eta_1 e^{-t_1 \dot{\gamma}}$, of the viscosity is considered — the "plastic" part, $\tau_0/\dot{\gamma}$, is omitted.

What is immediately striking in Fig. 2 is that $\tau(\dot{\gamma})$ is not a strictly increasing function, but has a maximum of $\tau_m = \tau_0 + \eta_1 \dot{\gamma}_1/e$ at $\dot{\gamma} = \dot{\gamma}_1$. This is due to the excessive shear-thinning for $\dot{\gamma} > \dot{\gamma}_1$, which causes not only the viscosity, but even the stress itself, to fall. This has the following repercussions.

Firstly, the stress cannot increase beyond the value τ_m. This means that there are many cases for which steady-state solutions do not exist because the momentum balance would require higher stress values than the model can provide. One example is Poiseuille flows whose pressure gradient exceeds a certain threshold, a case that will be examined shortly.

Secondly, for those cases that a solution exists, we can see that the same stress state can be achieved with two different values of the

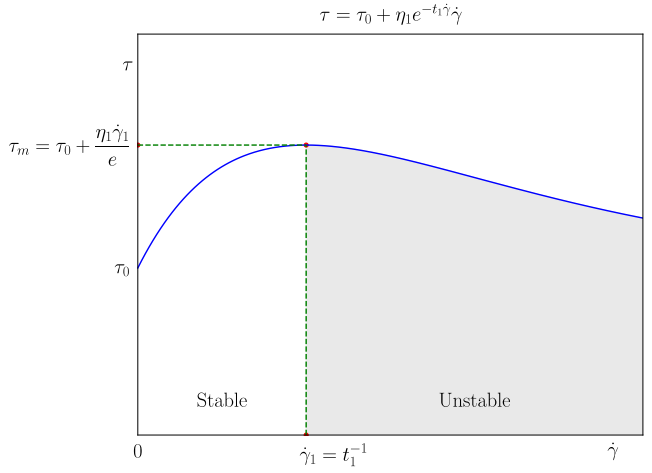

Fig. 2. Variation of stress with the strain rate, for the De Kee model.

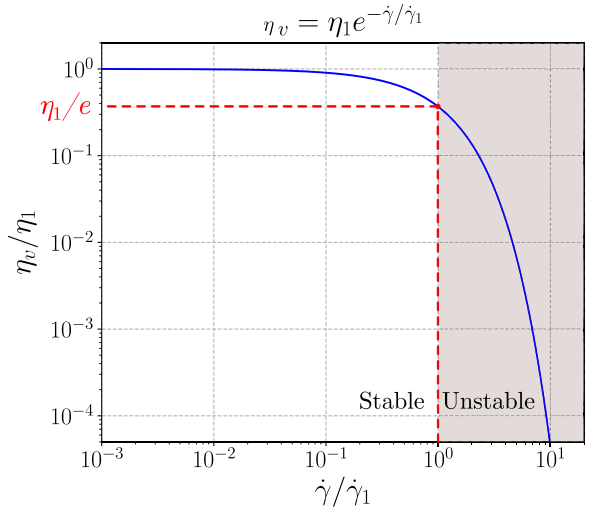

Fig. 3. Variation of the "viscous" component of the viscosity, $\eta_1 e^{-t_1\dot{\gamma}}$, with the strain rate. The viscosity is normalised by η_1 and the strain rate by $\dot{\gamma}_1 = t_1^{-1}$.

shear rate — that is, for each value of $\tau \in (\tau_0, \tau_m)$ the corresponding horizontal line in Fig. 2 intersects the $\tau(\dot{\gamma})$ curve at two points, say $\dot{\gamma}_- < \dot{\gamma}_0$ and $\dot{\gamma}_+ > \dot{\gamma}_0$. Hence, we expect multiple solutions, when they exist. Of these solutions, those with shear rates $\dot{\gamma} > \dot{\gamma}_0$ will be unstable because any perturbation in $\dot{\gamma}$ will cause the stress to change in such a direction that will amplify further the change in the shear rate, starting a vicious circle. If $\dot{\gamma}$ is increased, τ falls and the reduced viscous resistance in the fluid will cause a further increase in $\dot{\gamma}$ and so on. The opposite will happen if $\dot{\gamma}$ is perturbed in the negative direction: this will cause τ to increase, strengthening the viscous resistance to the flow and causing further decrease to $\dot{\gamma}$ etc. A formal stability analysis showing that solutions corresponding to a negative-slope branch of a steady-state flow curve are unstable has been reported in the early work of Yerushalmi et al. (1970). These features of the model will be demonstrated in the case of planar Poiseuille flow in the next section.

Concerning the viscosity, Fig. 3 seems like a typical shear-thinning viscosity curve. At low shear rates, $\dot{\gamma} \ll \dot{\gamma}_1$, the "viscous" contribution to the viscosity, $\eta_1 e^{-\dot{\gamma}/\dot{\gamma}_1}$, is approximately constant and equal to η_1, with the model exhibiting an almost Newtonian behaviour, in contrast to the $k\dot{\gamma}^{n-1}$ component of the HB viscosity which becomes infinite at vanishing shear rate. At $\dot{\gamma} = \dot{\gamma}_1$ this viscosity component has decreased to $\eta_v = \eta_1/e \approx 0.37\eta_1$. Beyond $\dot{\gamma} = \dot{\gamma}_1$ the shear thinning intensifies dramatically. However, it should be noted that $\dot{\gamma} > \dot{\gamma}_1$ lies in the unstable regime and therefore the lowest practically achievable viscosity is $\eta_v = \eta_1/e \approx 0.37\eta_1$ with viscosities lower than that being practically impossible to achieve in steady flow. In other words, practically $\eta_v \in [0.37\eta_1, \eta_1]$.

Table 1
Parameters of the model (2) as fitted to rheological data for various real fluid by De Kee and Turcotte (1980). The last two columns list the critical rate of strain and the maximum attainable stress, respectively (Fig. 2).

	τ_0 [Pa]	η_1 [Pa.s]	t_1 [s]	$\dot{\gamma}_1$ [1/s]	τ_m [Pa]
Banana puree	1.04×10^2	6.26×10^4	6.23×10^1	1.61×10^{-2}	4.74×10^2
Blood	3.81×10^{-3}	7.17×10^{-3}	3.29×10^{-2}	3.04×10^1	8.40×10^{-2}
Mayonnaise	1.35×10^2	4.20×10^{-1}	1.44×10^{-4}	6.94×10^3	1.21×10^3
Yogurt	4.17×10^1	1.15×10^{-2}	4.52×10^{-5}	2.21×10^4	1.35×10^2

To give a feel of the practical range of applicability of the model, Table 1 lists the values of its parameters as fitted to rheological data for various real fluids by De Kee and Turcotte (1980), together with the corresponding values of critical rate of strain $\dot{\gamma}_1$ and maximum attainable stress τ_m.

It is perhaps useful to note that a constitutive model can have a monotonically increasing yield curve which is, at the same time, bounded. For example, regularised versions of the Bingham constitutive model with zero plastic viscosity have been proposed and used for the plastic flow of ductile solids (Bašić et al., 2005) and for viscoplastic fluids (Garimella et al., 2022) (the model (Garimella et al., 2022) is equivalent to the Papanastasiou-regularised Bingham model with zero plastic viscosity). In such cases the monotonicity allows the existence of stable solutions for all values of the shear rate. On the other hand, the boundedness means again that there are cases for which steady-state solutions do not exist because they would require higher stresses than the model can provide. This can be the case for flow configurations that are defined in terms of specified dynamics (e.g. Poiseuille flow under a specified pressure gradient), whereas cases defined in terms of specified kinematics (e.g. Poiseuille flow under imposed flow rate or Couette flow under specified wall velocity) would be solvable. But the subject of our present investigation, the De Kee–Turcotte model, has a flow curve that is both bounded and non-monotonic.

4. Planar Poiseuille flow

With these considerations, let us proceed to the analytical solution of planar Poiseuille flow.

4.1. Preliminary considerations

For simple shear flow, the De Kee model (2) reduces to the following form:

$$\begin{cases} \dfrac{du}{dy} = 0 & |\tau_{yx}| < \tau_0 \\ \tau_{yx} = \left(\dfrac{\tau_0}{|du/dy|} + \eta_1 e^{-\frac{|du/dy|}{\dot{\gamma}_1}} \right) \dfrac{du}{dy} & |\tau_{yx}| \geq \tau_0 \end{cases} \tag{7}$$

where x is the flow direction and u is the velocity in that direction, y is the perpendicular direction across which $u(y)$ varies, and τ_{yx} is the shear stress.

One such flow is planar Poiseuille flow, a steady flow where fluid is pushed along a channel formed by two infinite horizontal parallel plates, located at a distance $2H$ apart, by an imposed pressure gradient, $G = -dp/dx$ (Fig. 4). For this flow, the momentum balance (Cauchy equation) reduces to:

$$\tau_{yx} = -Gy \tag{8}$$

where $y = 0$ is set midway between the plates (Fig. 4). The stress grows linearly with distance from the midplane, ranging from zero at the midplane to a maximum magnitude of GH at the plates. Therefore,

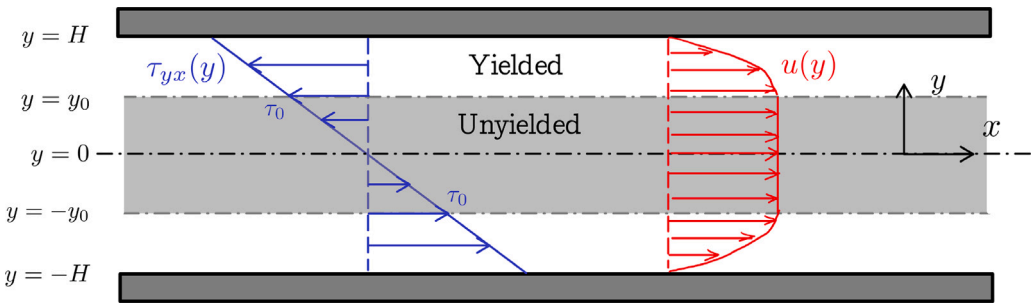

Fig. 4. Sketch of the configuration of viscoplastic planar Poiseuille flow.

as long as $\tau_0 \neq 0$, an unyielded core will form in the middle of the domain, up to a distance of

$$y_0 = \frac{\tau_0}{G} \tag{9}$$

from the midplane (from Eq. (8)). If $y_0 > H$ then obviously no flow will occur and the whole material will be unyielded, provided that no-slip conditions apply at the plates, which is an assumption that will be made in the present paper. Otherwise, if $y_0 < H$, then there will be a yielded zone in $y \in [y_0, H]$ and flow will occur. We can therefore focus on the partially yielded case and first consider the yielded zone, where we can substitute Eq. (7) in Eq. (8); in the upper half ($y > 0$) of the domain, where $du/dy < 0$, this substitution gives

$$\left(\frac{\tau_0}{-du/dy} + \eta_1 \, e^{\frac{du/dy}{\dot\gamma_1}} \right) \frac{du}{dy} = -Gy \tag{10}$$

This can be easily manipulated into the form

$$\frac{1}{\dot\gamma_1} \frac{du}{dy} e^{\frac{1}{\dot\gamma_1}\frac{du}{dy}} = \frac{\tau_0 - Gy}{\eta_1 \dot\gamma_1} \tag{11}$$

Applying the Lambert function to both sides and rearranging we get

$$\frac{du}{dy} = \dot\gamma_1 W\left(\frac{\tau_0 - Gy}{\eta_1 \dot\gamma_1} \right) \tag{12}$$

The left-hand side, du/dy, is negative, and hence the output of the Lambert function on the right-hand side must also be negative, which requires that its argument is negative (Fig. 1). This is indeed the case, as the occurrence of flow means that $Gy > \tau_0$ (Eq. (8)). But this means that we are in the region where W has two branches, and hence there are two solutions to Eq. (12), one employing W_0 and one employing W_{-1}. We will examine this issue later, but for now let us proceed without particularising the branch that is selected.

According to what was said in Section 2, in order for Eq. (12) to have a solution, the argument of the Lambert function must be greater than or equal to $-1/e$. This argument is negative, and its magnitude is maximised at $y = H$. Therefore, the existence of a solution requires that

$$-\frac{1}{e} \leq \frac{\tau_0 - GH}{\eta_1 \dot\gamma_1} \quad \Leftrightarrow \quad GH \leq \tau_0 + \frac{\eta_1 \dot\gamma_1}{e} \tag{13}$$

Now, from Eq. (8), GH is the maximum stress value, required at the plates so that the pressure gradient is counterbalanced and the flow is steady. Therefore, Eq. (13) is equivalent to the condition

$$\tau_{xy}(y = H) \leq \tau_0 + \frac{\eta_1 \dot\gamma_1}{e} \equiv \tau_m \tag{14}$$

which simply says that the stress should be everywhere smaller than the maximum value τ_m producible by the De Kee–Turcotte model, as shown in Section 3. If the pressure gradient G is too large for τ_m to counteract it (i.e. condition (13) is not satisfied), then steady-state flow is not possible.

4.2. Velocity profile

Assuming that the pressure gradient is sufficiently small to satisfy condition (13), we will proceed with the integration of Eq. (12). For convenience, it will be brought to non-dimensional form by employing the following non-dimensionalisation:

$$\tilde u = \frac{u}{\dot\gamma_1 H} \quad , \quad \tilde y = \frac{y}{H} \Rightarrow \frac{d}{dy} = \frac{1}{H}\frac{d}{d\tilde y} \quad , \quad \tilde G = \frac{GH}{\eta_1 \dot\gamma_1} \tag{15}$$

We will also substitute $\tau_0 = Gy_0$ (Eq. (9)). The non-dimensional form of (12) is then:

$$\frac{d\tilde u}{d\tilde y} = W\left(\tilde G(\tilde y_0 - \tilde y) \right) \tag{16}$$

This can be integrated using Eq. (4), while the constant of integration can be determined by the boundary condition $\tilde u(H) = 0$, to arrive at the following velocity profile for the yielded region:

$$\begin{aligned} \tilde u = {} & (\tilde y - \tilde y_0)\left[W\left(\tilde G\left(\tilde y_0 - \tilde y \right) \right) - 1 \right] - (1 - \tilde y_0)\left[W\left(\tilde G\left(\tilde y_0 - 1 \right) \right) - 1 \right] \\ & + \frac{1}{\tilde G}\left[e^{W(\tilde G(\tilde y_0 - 1))} - e^{W(\tilde G(\tilde y_0 - \tilde y))} \right] , \qquad \tilde y \in [\tilde y_0, 1] \end{aligned} \tag{17}$$

In the unyielded region the velocity is uniform and equal to that of the yielded region at $\tilde y = \tilde y_0$:

$$\begin{aligned} \tilde u = {} & \frac{1}{\tilde G}\left[e^{W(\tilde G(\tilde y_0 - 1))} - e^{W(0)} \right] \\ & - (1 - \tilde y_0)\left[W\left(\tilde G\left(\tilde y_0 - 1 \right) \right) - 1 \right] , \qquad \tilde y \in [0, \tilde y_0] \end{aligned} \tag{18}$$

At this point, it is pertinent to consider the issue of the branches of W. Returning to Eq. (12), we note the following.

Principal branch

For $x \leq 0$, $W_0(x) \in [-1, 0]$, so that it follows from Eq. (12) that $|du/dy| \leq \dot\gamma_1$ and we are in the stable region of Fig. 2.

With increasing y, i.e. closer to the wall, the argument $(\tau_0 - Gy)/\eta_1\dot\gamma_1$ of W in Eq. (12) becomes more negative, and hence $|W_0(\cdot)|$ increases (Fig. 1), implying that $|du/dy|$ also increases (Eq. (12)). This is normal behaviour: higher velocity gradients develop near the walls; it is because higher stresses require higher velocity gradients in the stable region.

On the other hand, considering what happens when $y \to y_0$, due to Eq. (9) the argument of W_0 in Eq. (12) tends to zero, and so does $W_0(\cdot)$ itself, so that the velocity gradient is zero at the yield surface — again, normal behaviour exhibited by other viscoplastic models as well. Stress continuity at the yield surface requires that the viscous part of the stress decreases towards zero, leaving only the plastic part, as we approach the yield surface from the yielded side.

Velocity profiles for cases without yield stress ($\tilde y_0 = 0$) and with yield stress ($\tilde y_0 = 0.5$) are shown in Figs. 5(a) and 6(a), respectively, for various values of dimensionless pressure gradient $\tilde G$, up to the maximum allowable for steady-state attainment ($\tilde G_{\max} = 1/e$ for $\tilde y_0 = 0$

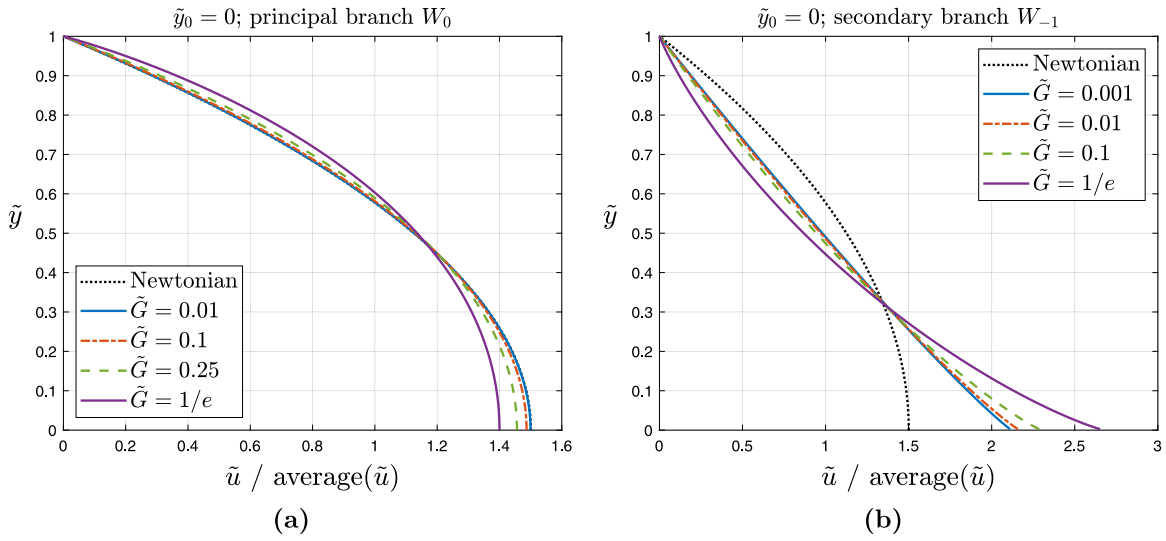

Fig. 5. Velocity profiles, normalised by the mean velocity, for $y_0 = 0$ (no yield stress), obtained with (a) W_0 (stable) and (b) W_{-1} (unstable).

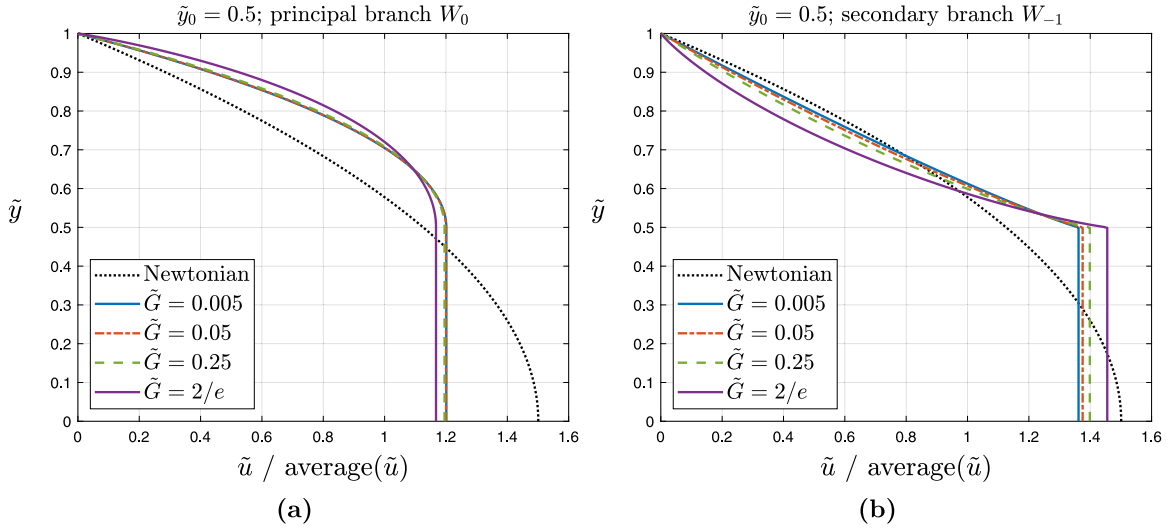

Fig. 6. Velocity profiles, normalised by the mean velocity, for $y_0 = 0.5$ obtained with (a) W_0 (stable) and (b) W_{-1} (unstable).

and $\tilde{G}_{\max} = 2/e$ for $\tilde{y}_0 = 0.5$). The maximum allowable dimensionless pressure gradient is obtained by substituting $\tau_0 = G y_0$ in the condition (13) and non-dimensionalising it to get:

$$\tilde{G}\left(1 - \tilde{y}_0\right) \leq \frac{1}{e} \tag{19}$$

Secondary branch

Since $W_{-1}(\cdot) \leq -1$, it follows from Eq. (12) that $|du/dy| \geq \dot{\gamma}_1$ and we are in the unstable region of Fig. 2.

With increasing y, i.e. closer to the wall, the argument $(\tau_0 - Gy)/\eta_1\dot{\gamma}_1$ of W in Eq. (12) becomes more negative, and hence $|W_{-1}(\cdot)|$ *decreases* (Fig. 1), implying that $|du/dy|$ *decreases as well* (Eq. (12)). This is the opposite of what is normally expected, but due to $\tau_{yx}(\dot{\gamma})$ being a decreasing function in the unstable region (Fig. 2), in order to get the needed higher stresses near the wall the shear rate has to decrease there.

Again counterintuitively, when $y \to y_0$, due to Eq. (9) the argument of W_{-1} in Eq. (12) tends to zero, and $W_{-1}(\cdot)$ tends to $-\infty$, so that the velocity gradient becomes infinite at the yield surface.

Velocity profiles for cases without yield stress ($\tilde{y}_0 = 0$) and with yield stress ($\tilde{y}_0 = 0.5$) are shown in Figs. 5(b) and 6(b), respectively, for various values of dimensionless pressure gradient $\tilde{G}$, up to the maximum allowable for steady-state attainment. Of course, these solutions are unstable. The plots seem to show finite values of the velocity gradient (16) at $\tilde{y} \to \tilde{y}_0$ instead of the theoretical infinite one, but this is due to the slowness of the decrease of $W_{-1}(x)$ towards $-\infty$ as $x \to 0$. For example, for $\tilde{y}_0 - \tilde{y} = 0.001$, which is a typical $\tilde{y}$-value resolution for drawing the plots, Eq. (16) gives a dimensionless velocity gradient $d\tilde{u}/d\tilde{y}$ of -14.2 for $\tilde{G} = 0.01$ and -11.7 for $\tilde{G} = 0.1$ (note also that the slopes in Figs. 5(b) and 6(b) are not to scale, because the velocities have been normalised by their average values).

4.3. Flow rate

When a solution exists, the flow rate, per unit width, can be calculated by integrating the velocity across the height of the channel:

$$Q = \int_{y=-H}^{y=+H} u\,dy = 2\int_{y=0}^{y=H} u\,dy \tag{20}$$

where the symmetry about the $y = 0$ plane has been exploited. Also, it will be convenient to non-dimensionalise the flow rate:

$$\tilde{Q} \equiv \frac{Q}{2\dot{\gamma}_1 H^2} = \int_{\tilde{y}=0}^{\tilde{y}=\tilde{y}_0} \tilde{u}_0\,d\tilde{y} + \int_{\tilde{y}=\tilde{y}_0}^{\tilde{y}=1} \tilde{u}\,d\tilde{y} \tag{21}$$

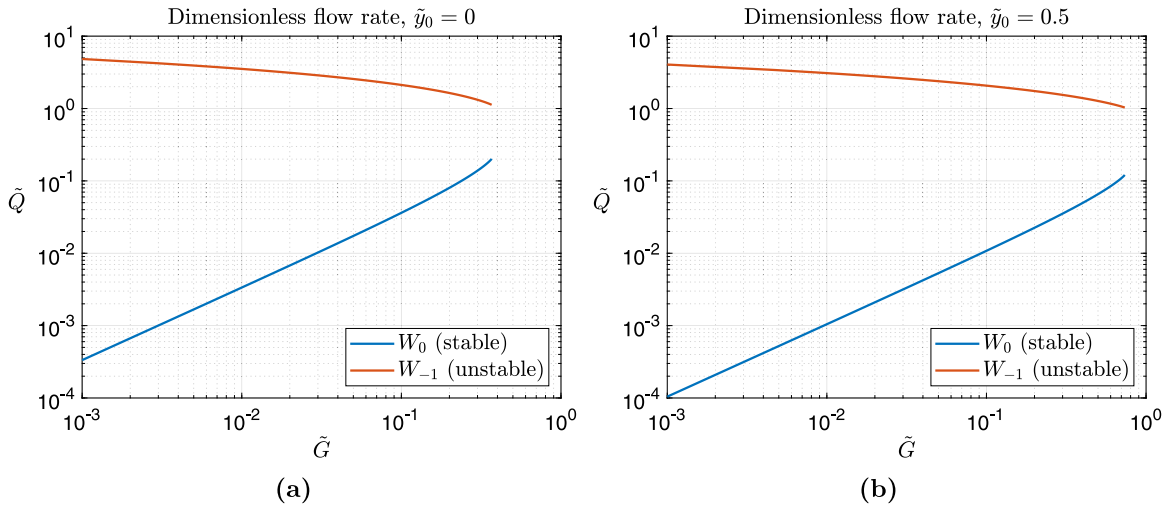

Fig. 7. Plots of dimensionless flow rate $\tilde{Q}$ as a function of the dimensionless pressure gradient $\tilde{G}$, for the case that the fluid has no yield stress (a) and for the viscoplastic case with $\tilde{y}_0$ held at 0.5 (b).

where, for convenience, the steady velocity (18) of the unyielded plug is denoted as $\tilde{u}_0$. With this notation, the velocity in the yielded region can be written as

$$\tilde{u} = \tilde{u}_0 + \left(\tilde{y} - \tilde{y}_0\right)\left[W\left(\tilde{G}\left(\tilde{y}_0 - \tilde{y}\right)\right) - 1\right] - \frac{1}{\tilde{G}} e^{W(\tilde{G}(\tilde{y}_0 - \tilde{y}))} + \frac{1}{\tilde{G}} e^{W(0)}, \quad \tilde{y} \in [\tilde{y}_0, 1] \tag{22}$$

and the above integral becomes

$$\tilde{Q} = \tilde{u}_0 + \frac{1 - \tilde{y}_0}{\tilde{G}} e^{W(0)} + \int_{\tilde{y}=\tilde{y}_0}^{\tilde{y}=1} \left(\tilde{y} - \tilde{y}_0\right)\left[W\left(\tilde{G}\left(\tilde{y}_0 - \tilde{y}\right)\right) - 1\right] d\tilde{y} - \frac{1}{\tilde{G}} \int_{\tilde{y}=\tilde{y}_0}^{\tilde{y}=1} e^{W(\tilde{G}(\tilde{y}_0 - \tilde{y}))} d\tilde{y} \tag{23}$$

This can be evaluated with the help of Eqs. (5) and (6), to obtain

$$\tilde{Q} = \tilde{u}_0 + \frac{1 - \tilde{y}_0}{\tilde{G}} e^{W(0)} + \frac{1}{8\tilde{G}^2}\left[\left(2\varpi^2 + 1\right)(2\varpi - 1)\, e^{2\varpi} + e^{W(0)}\right] - \frac{(1 - \tilde{y}_0)^2}{2} + \frac{1}{4\tilde{G}^2}\left[(2\varpi + 1)\, e^{2\varpi} - e^{W(0)}\right] \tag{24}$$

where $\varpi = W(\tilde{G}(\tilde{y}_0 - 1))$. Because $W_0(0) = 0$ and $W_{-1}(0) = -\infty$, the term $e^{W(0)}$ equals 1 for the stable branch and 0 for the unstable one. Fig. 7 shows plots of the dimensionless flow rate $\tilde{Q}$ as a function of the dimensionless pressure gradient $\tilde{G}$ for $\tilde{y}_0 = 0$ (no yield stress) and $\tilde{y}_0 = 0.5$. Note that in the latter case, since $\tilde{y}_0 = 0.5$ is held constant in Fig. 7(b) irrespective of $\tilde{G}$, the curve $\tilde{Q} = f(\tilde{G})$ should not be construed as varying the pressure gradient in a fixed channel with a fixed fluid, but in order for $\tilde{y}_0$ to remain constant as the pressure gradient varies the yield stress of the fluid must vary simultaneously with $\tilde{G}$ (from Eq. (9) we get $\tilde{y}_0 = \tilde{\tau}_0/\tilde{G}$ where $\tilde{\tau}_0 = \tau_0/\eta_1\dot{\gamma}_1$).

5. Conclusions

The De Kee–Turcotte model has the advantages of the physical significance of its parameters and its viscous plateau at low shear rates. On the other hand, its exponential shear-thinning limits its range of applicability: it bounds the magnitude of the stress that it can produce, making it unusable in high-stress flows. Furthermore, its flow curve exhibits a maximum which splits it into a stable (stress-increasing) part and an unstable (stress-decreasing) part. The behaviour of the model in the stable region is akin to the other simple viscoplastic models, such as the Herschel–Bulkley. An analytical solution was given for planar Poiseuille flow in terms of the Lambert W function.

Ironically, the model's exponential shear-thinning behaviour with the resulting limitation that it imposes on the model allows solutions only in cases with mild shear-thinning. Hence, the velocity profiles in Figs. 5(a) and 6(a) are reminiscent of mildly shear-thinning power-law and Herschel–Bulkley profiles. However, power-law and Herschel–Bulkley fluids can undergo much more shear-thinning than a De Kee fluid. In any case the viscosity $\eta_1 e^{-t_1\dot{\gamma}}$ cannot drop below $1/e \approx 36.8\%$ of its zero-shear-rate value η_1 if we are to remain in the stable region (Fig. 3).

One can try to increase the range of applicability by decreasing the time constant t_1 (increasing the critical rate of strain $\dot{\gamma}_1$), but this will expand the Newtonian plateau (Fig. 3) making the fluid more Newtonian (or more Bingham-like in the viscoplastic case). On the other hand, another possibility for extending the model's range of applicability would be to incorporate multiple viscous components $\sum_i \eta_i e^{-t_i\dot{\gamma}}$ (De Kee and Turcotte, 1980; Kaczmarczyk et al., 2023). Also, we did not discuss the shear-thickening case, which is achieved by using negative time constants $t_1 < 0$ (critical rates-of-strain $\dot{\gamma}_1 < 0$). In this case the stress can grow without bound and the limitation vanishes. For the Poiseuille flow, this has the implication that in Eq. (12) the argument of the W function is now positive and therefore there are no limitations concerning its magnitude (Fig. 1).

The non-monotonicity of the De Kee flow curve establishes the existence of unstable solutions alongside the stable ones, whenever there are solutions at all. The unstable velocity profiles in planar Poiseuille flow were seen to exhibit inverted and unrealistic features compared to the stable ones.

CRediT authorship contribution statement

Alexandros Syrakos: Writing – review & editing, Writing – original draft, Supervision, Investigation, Formal analysis. **Aggelos Charalambous:** Investigation, Formal analysis. **Georgios C. Georgiou:** Writing – review & editing, Investigation, Formal analysis, Conceptualization.

Declaration of competing interest

The authors declare that they have no known competing financial interests or personal relationships that could have appeared to influence the work reported in this paper.

Data availability

No data was used for the research described in the article.

References

Balmforth, N.J., Frigaard, I.A., Ovarlez, G., 2014. Yielding to stress: Recent developments in viscoplastic fluid mechanics. Annu. Rev. Fluid Mech. 46, 121–146.

Bašić, H., Demirdžić, I., Muzaferija, S., 2005. Finite volume method for simulation of extrusion processes. Internat. J. Numer. Methods Engrg. 62 (4), 475–494.

Bingham, E.C., 1922. Fluidity and Plasticity. McGraw-Hill.

Bonn, D., Denn, M.M., Berthier, L., Divoux, T., Manneville, S., 2017. Yield stress materials in soft condensed matter. Rev. Modern Phys. 89.

Casson, N., 1959. Flow equation for pigment-oil suspensions of the printing ink-type. Rheol. Dispers. Syst. 84–104.

Corless, R.M., Gonnet, G.H., Hare, D.E., Jeffrey, D.J., Knuth, D.E., 1996. On the Lambert W function. Adv. Comput. Math. 5, 329–359.

Coussot, P., 2017. Bingham's heritage. Rheol. Acta 56, 163–176.

De Kee, D., Turcotte, G., 1980. Viscosity of biomaterials. Chem. Eng. Commun. 6 (4–5), 273–282.

Dimitriou, C.J., McKinley, G.H., 2019. A canonical framework for modeling elasto-viscoplasticity in complex fluids. J. Non-Newton. Fluid Mech. 265, 116–132.

Dinkgreve, M., Denn, M.M., Bonn, D., 2017. "Everything flows?": elastic effects on startup flows of yield-stress fluids. Rheol. Acta 56 (3), 189–194.

Frigaard, I., 2019. Simple yield stress fluids. Curr. Opin. Colloid Interface Sci. 43, 80–93.

Garimella, S.M., Anand, M., Rajagopal, K.R., 2022. A new model to describe the response of a class of seemingly viscoplastic materials. Appl. Math. 67 (2), 153–165.

Herschel, W.H., Bulkley, R., 1926. Konsistenzmessungen von Gummi-Benzollösungen. Kolloid-Zeitschrift 39, 291–300.

Huilgol, R.R., Georgiou, G.C., 2022. Fluid Mechanics of Viscoplasticity. Springer International Publishing.

Kaczmarczyk, K., Kruk, J., Ptaszek, P., Ptaszek, A., 2023. Plantago ovata husk: An investigation of raw aqueous extracts. Osmotic, hydrodynamic and complex rheological characterisation. Molecules 28 (4), 1660.

Larson, R.G., Wei, Y., 2019. A review of thixotropy and its rheological modeling. J. Rheol. 63 (3), 477–501.

Mitsoulis, E., Tsamopoulos, J., 2017. Numerical simulations of complex yield-stress fluid flows. Rheol. Acta 56 (3), 231–258.

Moschopoulos, P., Varchanis, S., Syrakos, A., Dimakopoulos, Y., Tsamopoulos, J., 2022. S-PAL: A stabilized finite element formulation for computing viscoplastic flows. J. Non-Newton. Fluid Mech. 309, 104883.

Papanastasiou, T.C., 1987. Flows of materials with yield. J. Rheol. 31 (5), 385–404.

Pitsillou, R., Georgiou, G.C., Huilgol, R.R., 2020a. On the use of the Lambert function in solving non-Newtonian flow problems. Phys. Fluids 32 (9).

Pitsillou, R., Syrakos, A., Georgiou, G.C., 2020b. Application of the Lambert W function to steady shearing Newtonian flows with logarithmic wall slip. Phys. Fluids 32 (5).

Saramito, P., 2009. A new elastoviscoplastic model based on the Herschel–Bulkley viscoplastic model. J. Non-Newton. Fluid Mech. 158 (1–3), 154–161.

Saramito, P., Wachs, A., 2017. Progress in numerical simulation of yield stress fluid flows. Rheol. Acta 56 (3), 211–230.

Seo, Y.P., Choi, H.J., Seo, Y., 2011. Analysis of the flow behavior of electrorheological fluids with the aligned structure reformation. Polymer 52 (25), 5695–5698.

Sverdrup, K., Nikiforakis, N., Almgren, A., 2018. Highly parallelisable simulations of time-dependent viscoplastic fluid flow with structured adaptive mesh refinement. Phys. Fluids 30 (9).

Syrakos, A., Dimakopoulos, Y., Tsamopoulos, J., 2020. A finite volume method for the simulation of elastoviscoplastic flows and its application to the lid-driven cavity case. J. Non-Newton. Fluid Mech. 275, 104216.

Varchanis, S., Makrigiorgos, G., Moschopoulos, P., Dimakopoulos, Y., Tsamopoulos, J., 2019. Modeling the rheology of thixotropic elasto-visco-plastic materials. J. Rheol. 63 (4), 609–639.

Wang, W., De Kee, D., Khismatullin, D., 2011. Numerical simulation of power law and yield stress fluid flows in double concentric cylinder with slotted rotor and vane geometries. J. Non-Newton. Fluid Mech. 166 (12–13), 734–744.

Yahia, A., Khayat, K., 2001. Analytical models for estimating yield stress of high-performance pseudoplastic grout. Cem. Concr. Res. 31 (5), 731–738.

Yerushalmi, J., Katz, S., Shinnar, R., 1970. The stability of steady shear flows of some viscoelastic fluids. Chem. Eng. Sci. 25 (12), 1891–1902.

Zare, Y., Rhee, K.Y., 2019. Modeling of viscosity and complex modulus for poly (lactic acid)/poly (ethylene oxide)/carbon nanotubes nanocomposites assuming yield stress and network breaking time. Composites B 156, 100–107.

Zhu, H., De Kee, D., 2007. A numerical study for the cessation of couette flow of non-Newtonian fluids with a yield stress. J. Non-Newton. Fluid Mech. 143 (2–3), 64–70.

Zhu, H., Kim, Y., De Kee, D., 2005. Non-Newtonian fluids with a yield stress. J. Non-Newton. Fluid Mech. 129 (3), 177–181.